

536128

To be Submitted to the ApJ

The *CHANDRA* HETGS X-ray Grating Spectrum of η Carinae

M. F. Corcoran^{1,2}, J. H. Swank², R. Petre², K. Ishibashi³, K. Davidson⁴, L. Townsley⁵, R. Smith⁶, S. White⁷, R. Viotti⁸, A. Damini⁹

ABSTRACT

η Carinae may be the most massive and luminous star in the Galaxy and is suspected to be a massive, colliding wind binary system. The *CHANDRA* X-ray observatory has obtained a calibrated, high-resolution X-ray spectrum of the star uncontaminated by the nearby extended soft X-ray emission. Our 89 ksec *CHANDRA* observation with the High Energy Transmission Grating Spectrometer (HETGS) shows that the hot gas near the star is non-isothermal. The temperature distribution may represent the emission on either side of the colliding wind bow shock, effectively “resolving” the shock. If so, the pre-shock wind velocities are ~ 700 and ~ 1800 km s⁻¹ in our analysis, and these velocities may be interpreted as the terminal velocities of the winds from η Carinae and from the hidden companion star. The forbidden-to-intercombination (*f/i*) line ratios for the He-like ions of S, Si and Fe are large, indicating that the line forming region lies far from the stellar photosphere. The iron fluorescent line at 1.93Å, first detected by *ASCA*, is clearly resolved from the thermal iron line in the *CHANDRA* grating spectrum. The Fe fluorescent line is weaker in our *CHANDRA* observation than in any of the *ASCA* spectra. The *CHANDRA* observation also provides the first high-time resolution lightcurve of the uncontaminated stellar X-ray emission from η Carinae and shows that there is no significant, coherent variability during the *CHANDRA* observation. The η Carinae *CHANDRA* grating spectrum is unlike recently published X-ray grating spectra of single massive stars in significant ways and is generally consistent with colliding wind emission in a massive binary.

¹Universities Space Research Association, 7501 Forbes Blvd, Ste 206, Seabrook, MD 20706

²Laboratory for High Energy Astrophysics, Goddard Space Flight Center, Greenbelt MD 20771

³National Research Council, Laboratory For Astronomy and Space Physics, Goddard Space Flight Center, Greenbelt, MD 20771

⁴Astronomy Department, University of Minnesota, Minneapolis, MN, 55455

⁵Department of Astronomy, Pennsylvania State University, State College, PA

⁶Harvard-Smithsonian Center for Astrophysics, Cambridge, MA

⁷Department of Astronomy, University of Maryland, College Park, MD, 20742

⁸Istituto di Astrofisica Spaziale, CNR, Area di Ricerca Tor Vergata, 00133 Roma, Italy

⁹Instituto Astronômico e Geofísico da USP, Av. Miguel Stefano 4200, 04301-904 São Paulo, Brazil

Subject headings: η Carinae, stars: individual (η Carinae), stars: early-type, X-rays:stars, binaries: general

1. Introduction

The superluminous star η Carinae has been observed by nearly every X-ray satellite flown. *EINSTEIN* observations (Seward et al. 1979; Seward and Chlebowski 1982; Chlebowski et al. 1984) first resolved the star's X-ray emission from the rest of the Carina Nebula and mapped out point-like emission centered on the star and an elliptical X-ray ring around the star extending out to $\sim 15''$. *GINGA* (Koyama et al. 1990) and *BBXRT* provided the first clear measures of the strong Fe K line indicative of thermal emission probably produced by shocked gas. *ROSAT* discovered the variable nature of the hard source (Corcoran et al. 1995), while *ASCA* discovered $\geq 50\times$ solar abundance of nitrogen (Tsuboi et al. 1997) in the outer homunculus and fluorescent Fe K emission (Corcoran et al. 1998) unresolved from the strong thermal line. A 2-10 keV X-ray lightcurve obtained by *RXTE* (consisting typically of 1 observation per week since 1996) revealed small amplitude periodic flares with $P = 85$ days (Corcoran et al. 1997) and confirmed that the variability seen in 1992 by *ROSAT* recurred (Ishibashi et al. 1999; Corcoran et al. 2001) on the same 5.5 year period which fits the He I 10830Å line variability reported by Daminieli (1996). These recent X-ray measurements along with variations in the radio (Duncan et al. 1995) and near-IR (Daminieli et al. 2000) all suggest that η Carinae may be the Galaxy's most massive binary system (Daminieli, Conti and Lopes 1997; Corcoran et al. 2001) in which the hard X-ray emission is produced by shocked gas in the region where the wind from η Carinae collides with the wind from the companion star. An early observation of η Carinae by the Advanced CCD Imaging Spectrometer (ACIS) on *CHANDRA* in September 1999 (Seward et al. 2001) provided the first image of the X-ray regions at a resolution of $\approx 1''$, though, due to degradation produced by charged particle damage of the CCDs, this observation could not be precisely calibrated spectrally.

Here we report the first calibrated observation of η Carinae with the High Energy Transmission Grating Spectrometer (HETGS, Canizares et al. 2001, in preparation) on the *CHANDRA* X-ray observatory (Weisskopf, O'Dell, & van Speybroeck 1996) using the ACIS linear array (ACIS-S) to read out the dispersed spectrum. The *CHANDRA* HETGS is well suited for observing the point-like hard emission from η Carinae for two reasons: 1) the spectral energy distribution of the emission fits nicely in the HETGS bandpass and 2) this emission is thought to be dominated by thermal processes which should produce strong line emission in the dispersed spectrum. Our deep (24.9 hour) observation of η Carinae with the HETGS provides the first spectrally-resolved measure of the X-ray spectrum, allowing for the first time a detailed definition of the temperature distribution, density, and chemical abundance of the hot, unresolved emission from the star. In this first report we discuss the overall spectral morphology of the unresolved X-ray emission, examine the emission line temperature and density diagnostics, and provide an uninterrupted lightcurve of the unresolved X-ray source over the length of the observation.

2. The Observation

The *CHANDRA* HETGS+ACIS-S observation of η Carinae was performed on 19 November 2000 – 20 November 2000. The total exposure time of the observation was 89,546 seconds. The spacecraft roll was chosen so as to avoid contamination of the dispersed spectra by other bright X-ray sources in the field. The data were cleaned and processed using the standard pipeline processing available at the *CHANDRA* X-ray Center. Images and spectra were extracted from the level 1.5 events using the Chandra Interactive Analysis of Observations (CIAO) analysis package.

The zeroth-order image, color-coded by X-ray energy is shown in figure 1. This image is similar to that previously published (Seward et al. 2001) though the energy calibration is better in the new image. In particular, the ACIS-S zeroth-order image shows the soft elliptical “shell” of emission surrounding the hard X-ray core, which is unresolved to ACIS at scales of $\sim 0.5'' \approx 10^{16}\text{cm} \approx 1000$ AU. The X-ray flux in the elliptical “shell” is very non-uniform, bright in the south and west (near the “S-ridge” and the “W-condensations” in the outer debris field, Walborn, Blanco & Thackeray 1978) and faint in the north and east. The hard, unresolved “core” appears to be surrounded by a halo of X-ray emission at moderate X-ray energies.

3. The X-ray Grating Spectrum of η Carinae

The ACIS-S image of the dispersed spectrum shows that the hard source is unresolved to *CHANDRA*; in particular, there is no observed dispersed spectrum from any other source of emission in the ACIS-S field aside from the unresolved, hard core source associated with η Carinae. We extracted the dispersed medium energy grating (MEG) and high energy grating (HEG) spectra from the X-ray event file using CIAO. Both plus and minus orders for the first, second and third order MEG and HEG source spectra were extracted, along with appropriate background spectra. Figure 2 shows the MEG +1 order spectrum, while figure 3 shows the HEG +1 order in the vicinity of the Fe K line. The MEG and HEG spectra of η Carinae represent the first X-ray spectra of this star uncontaminated by extended soft emission. The MEG spectrum shows very little emission from the unresolved source at energies less than 1.5 keV ($\lambda > 8.5 \text{ \AA}$) due to strong absorption, and reveals a significant X-ray continuum in the 1 – 8 \AA range and the presence of strong line emission from lines of S XV–XVI, Si XIII–XIV, Mg XII, Ca XIX, and Fe K. Strong forbidden lines of S XV, Si XIII and Mg XII were detected. In the HEG spectrum, the Fe line region shows a thermal emission line produced by Fe XXV and a blend of fluorescent Fe I $K\alpha_1+K\alpha_2$ lines centered at 1.94 \AA .

3.1. Modelling the Spectrum

We attempted to fit the MEG spectrum with a combination of optically-thin thermal emission models using the XSPEC analysis package (Arnaud 1996). Because the dispersed spectrum has

many bins with few counts and because background does not contribute significantly in the energy range of interest ($E > 1.5$ keV or $\lambda < 8$ Å), we used a modified version of the “C-statistic” (Cash 1979) on the total (non-background-subtracted) spectrum instead of the χ^2 statistic. Previous analyses indicated that the emission at energies above 1.5 keV could be fit by emission at a single temperature (for eg., Corcoran et al. 2000). As shown in Figures 4 and 5, a variable abundance single temperature thermal model (VMEKAL-XSPEC, Mewe, Kaastra & Liedahl 1995) provided a good fit to the continuum emission and most of the resolved emission lines. The parameters of the best fit single component model are given in Table 1. The single component temperature is $kT = 4.4$ keV with a column density of $N_H = 4.9 \times 10^{22}$ cm⁻², in reasonable agreement with earlier results. However, we found that no isothermal model could simultaneously match the strengths of the H-like and He-like lines of Si in the $4.5\text{Å} < \lambda < 6\text{Å}$ range. Fitting both the He-like and H-like ions required the addition of at least one additional thermal component. Our best fit 2-temperature model is given in table 2 and shown in figures 4 and 5. This 2-temperature model adequately matches the strength of both the He-like and H-like lines. This is the first time that an unresolved X-ray emission from η Carinae has been shown to require a non-isothermal temperature distribution. The maximum temperature we derive, $kT \approx 8.7$ keV, is nearly a factor of 2 larger than most other published temperatures for η Carinae, and to our knowledge represents the highest temperature ever associated with an early-type star.

In our modelling of the X-ray spectrum we held most elemental abundances at their solar values (Anders & Grevesse 1989), but allowed the abundances of Si, S and Fe (all of which have strong lines in the X-ray spectrum) to vary. The derived abundances for the 1 and 2 temperature models for these 3 elements are given in table 1. In each case the abundances of the Si, S, and Fe were slightly non-solar: Si needs was found to be slightly overabundant, S significantly overabundant (by about 70%), while Fe was slightly underabundant.

3.2. The He-like Lines and the f/i Ratio

The ratio of the intensity of the forbidden component to the intercombination component of the He-like lines (the f/i ratio) is a density diagnostic (Gabriel & Jordan 1969), though the ratio may be also increased by UV photoexcitation (Kahn et al. 2001) which can suppress the forbidden line and enhance the intercombination line. We fit the Si XIII, S XV and Fe XXV lines in XSPEC by first isolating the wavelength region around the line complex of interest and using gaussians to model the lines with inclusion of a power law component to describe the background. The fits are shown in figures 6–8 and the fit parameters are given in Table 2. The intercombination lines for all three ions are weak and our analysis only yields upper limits for the intensities of these lines. We measure f/i values of > 1.3 for Si XIII, > 2.0 for S XV and > 2.5 for Fe XXV. These values correspond to electron densities of $< 10^{14}$ cm⁻³ for Si XIII and $< 10^{15}$ cm⁻³ for S XV and Fe XXV.

3.3. The Fe Fluorescent Line

We fit the Fe I fluorescent line from the HEG spectrum in XSPEC by isolating the Fe K region and using a single gaussian line plus power-law background component. The line parameters are given in Table 1. The measured equivalent width of the line is only 39 eV, which is about half the value of the smallest equivalent width seen by *ASCA* (Corcoran et al. 2000).

4. The X-ray Lightcurve

From the zeroth-order image on the S3 chip we extracted a lightcurve in a circular 5'' diameter region centered on the unresolved source. We also extracted a background lightcurve from a source free circular region of diameter 17'' centered just beyond the outer elliptical emission region surrounding the hard unresolved source. We used bins of 1000 seconds for both the source and background lightcurve extraction; this yielded about 200 gross source counts and about 10-20 background counts in each bin. The background subtracted X-ray lightcurve of the unresolved source for the duration of the *CHANDRA* observation is shown in figure 9. This is the first uninterrupted lightcurve of the hard unresolved source spatially resolved from nearby contaminating emission. While there is some evidence for sporadic variability there is no evidence for coherent variations in the hard emission from the unresolved source during this observation.

5. Discussion

Recent evidence suggests that η Carinae may be a massive binary star, in which variable X-ray emission is produced by shocked gas at the interface where the wind from η Carinae collides with the wind of its companion (presumably some less massive early-type star). The line complexes resolved in the HETGS spectra provide unique information about the physical condition of the X-ray emitting region and thus on the single or binary nature of η Carinae. In the colliding wind model the wind from η Carinae forms a bow shock around the companion, since the companion's wind is probably weaker than η Carinae's wind, i.e. $\eta \equiv (\dot{M}V_\infty)_c / (\dot{M}V_\infty)_\eta < 1$; here \dot{M} represents the wind mass loss rate and V_∞ the wind terminal velocity, and the subscripts η and c refer to η Carinae and the companion, respectively. In published models (Damineli et al. 2000; Corcoran et al. 2001) the mass loss rate from η Carinae is thought to be at least a factor of 10 larger than that of the companion, while the terminal velocities are probably within a factor of 3 (see below), so that $\eta < 0.3$.

The mere presence of numerous strong emission lines confirms that the X-ray emission is dominated by thermal processes from shocked gas. The dominance of thermal processes in the *CHANDRA* energy range suggests that there is little or no contribution from non-thermal processes (which could be produced via inverse compton scattering of photospheric UV photons if Fermi

acceleration of the electron population in the shock is important). The temperature distribution of the X-ray emission as measured by *CHANDRA* provides a measure of the pre-shock wind velocities for both stars. In a colliding wind binary, the temperature of the shocked gas facing either star is kT (keV) $\approx 2.59\mu V^2$ (see the eq. 51 in Usov (1992)) where μ is the mean mass per particle and V is the stellar wind speed in 1000 km s⁻¹. For simplicity we assume $\mu \approx 1$, though this value may not be truly representative of the chemical composition of the wind of either η Carinae or its companion. We neglect the motion of the shock stagnation point due to the orbital motion of the stars, since orbital motion has a significant influence on the derived temperatures only when the stars are near periastron (and the stellar velocities are greatest), while the HETGS observation was obtained near apastron according to the ephemeris of Corcoran et al. (2001). The temperatures we derived, $kT \approx 1.1$ and ≈ 8.7 keV, suggest velocities of ~ 700 km s⁻¹ and ~ 1800 km s⁻¹. The speed of the wind from η Carinae is thought to be ~ 500 km s⁻¹ (Hillier et al. 2001), fairly consistent with the lower velocity we derive from our X-ray analysis. A velocity of ~ 500 km s⁻¹ is sufficient to produce the $kT \sim 1$ keV emission, but cannot produce the hotter emission revealed in the MEG spectrum. Naively, we interpret the low-temperature component as shocked emission from the relatively slow wind of η Carinae, and the high-temperature component as shocked emission by the faster wind from the companion star, so that $V_{\infty,\eta} \approx 700$ km s⁻¹ and $V_{\infty,c} \approx 1800$ km s⁻¹.

The f/i ratios derived from our analysis of the He-like ions are large, and show that the line forming region has a density $n_e < 10^{14}$ cm⁻³ and that enhancement of the intercombination component by UV photoexcitation is unimportant. This suggests that the line forming region is located far from the stellar photosphere, where wind densities and UV fluxes are low. This is broadly consistent with published descriptions of the orbit (Damineli et al. 2000; Corcoran et al. 2001) in which the shocked emission forms far from either star (though closer to the companion than to η Carinae) in a region of low particle and UV photon density. In the colliding wind model, the apex of the bow shock is located at a distance of $d/(1 + \sqrt{\eta})$ from η Carinae, where d is the separation of the two stars. At the phase of the *CHANDRA* observation, $\phi = 0.60$, the two stars are separated by about 4×10^{14} cm, using the orbital elements of Corcoran et al. (2001). At this time the bow shock is about 2.5×10^{14} cm from η Carinae, and about 1.5×10^{14} cm from the companion. The density of the wind at a distance r from the photosphere is $n = \dot{M}/(4\pi r^2 V \mu m_H)$, where \dot{M} is the mass loss rate and V the wind velocity. Using $\dot{M}_\eta = 10^{-4} M_\odot \text{ yr}^{-1}$ and $V_{\infty,\eta} \approx 500$ km s⁻¹ (Hillier et al. 2001), then the density of the wind from η Carinae at a distance of 2.5×10^{14} cm is only $n \approx 8 \times 10^8$ cm⁻³. Using $\dot{M}_c = 10^{-5} M_\odot \text{ yr}^{-1}$ (Corcoran et al. 2001) and $V_{\infty,c} = 1800$ km s⁻¹ as appropriate values for the companion's wind, the density of the companion's wind at a distance $r = 1.5 \times 10^{14}$ cm is also only about 10^8 cm⁻³. The predicted densities are consistent with the upper limits derived from our analysis of the f/i line intensity ratios. However, if the actual density of the emission region is near the limit implied by the f/i ratios, this might indicate that the assumed wind momentum balance is not quite right.

In contrast, newly published X-ray grating spectra of θ^1 Ori C (Schulz et al. 2000), ζ Ori (Waldron & Cassinelli 2001) and ζ Pup (Kahn et al. 2001) all have f/i ratios which are lower than

the values we derive from the η Carinae X-ray line spectrum. None of these stars are known to show any colliding wind effects, and apparently, in these massive stars, the X-ray lines form relatively near the stellar photosphere, probably within a few stellar radii. This is not the case for η Carinae.

The strength of the Fe fluorescent line is related to the column density of scattering material by $EW \approx 2.3N_{24}$ keV, where EW is the equivalent width of the line in keV and N_{24} the total column density of cold material in units of 10^{24} cm $^{-2}$ (Kallman 1995). The *ASCA* spectra suggest that $EW \approx 4 - 7N_{24}$ for η Carinae outside of eclipse (Corcoran et al. 2000). Thus at the time of the HETGS observation the equivalent width of the Fe fluorescent line implies $N_{24} \approx 0.01 - 0.03$, i.e. that the column density of cold material is $N_H \approx 1 - 3 \times 10^{22}$ cm $^{-2}$. This value is in fair agreement with the value of $N_H = 5 \times 10^{22}$ derived from fitting the X-ray continuum in the MEG spectrum, suggesting that some of the same material which produces the X-ray absorption also is responsible for producing the Fe fluorescent emission. The equivalent width of the line which we derive here is much smaller than any values given in either Corcoran et al. (2000) or Corcoran et al. (1998). This may be the result of the difficulty in determining the actual width of the fluorescent line in the *ASCA* spectra since the line is not resolved from the thermal component. However, if this variation is real, it may represent a real decrease in the scattering optical depth. Such a decrease is not unexpected in the binary model since at the time of the HETGS observation, the companion is nearly in front. Since the companion's wind is less dense this could produce a decrease in the scattering optical depth at the time of the HETGS observation.

6. Conclusions

We have presented here the first high-energy X-ray grating spectrum of the supermassive star η Carinae. This grating spectrum shows strong line emission from H-like and He-like ions of S, Si, Mg, Ca, and Fe, and confirms the presence of the Fe fluorescent line discovered by *ASCA*. The forbidden lines of the He-like ions are strong and the intercombination lines weak, indicating that the line forming region is far from the stellar photosphere. These results are all consistent with the current picture of η Carinae as a colliding wind binary. We expect that interesting variations in the X-ray spectrum will occur as the two stars approach periastron (which should next occur on June 20, 2003). In particular, we expect that the strength of the forbidden lines will weaken near periastron, as the density in the X-ray region increases and as the UV photospheric flux in the line region intensifies. Additional HETGS observations as the stars approach periastron, especially in conjunction with UV spectroscopy, will provide unique and significant constraints on the orbital geometry, the strengths of the winds from both stars, and the evolutionary stages of the stellar components.

We would like to thank the *CHANDRA* staff at the SAO/CfA and the HETGS team at MIT for their help in scheduling the observation and in analyzing the data. We made use of the FTOOLS suite of software supported by the HEASARC, and of the *ASCA* data archives also maintained at

the HEASARC. This research has made use of NASA's Astrophysics Data System Abstract Service.

REFERENCES

- Anders, E. & Grevesse, N., 1989, *Geochimica et Cosmochimica Acta*, 53, 197
- Arnaud, K. A., 1996, in *Astronomical Data Analysis Software and Systems V*, eds. Jacoby G. and Barnes J., p17, ASP Conf. Series volume 101.
- Chlebowski, T., et al., 1984, *ApJ*, 281, 665
- Cash, W. 1979, *ApJ*, 228, 939
- Corcoran, M. F., et al., 1995, *ApJ*, 445, L121
- Corcoran, M. F., et al., 1997, *Nature*, 390, 587
- Corcoran, M. F., et al., 1998, *ApJ*, 494, 381
- Corcoran, M. F., et al., 2000, *ApJ*, 545, 420
- Corcoran, M. F., Ishibashi, K., Swank, J. H., and Petre, R., 2001, *ApJ*, 547, 1034
- Damineli, A., 1996, *ApJ*, 460, L49
- Damineli, A., Conti, P. S., Lopes, D. F., 1997, *New Astronomy*, 2, 107
- Damineli, A., Lopes, D. F., and Conti, P. S., 1999, in *ASP. Conf. Ser. 179, η Carinae at the Millennium*, ed. J. A. Morse, R. M. Humphreys, and A. Damineli (San Francisco: ASP), 288
- Damineli, A., Kaufer, A., Wolf, B., Stahl, O., Lopes, D. F., Araújo, F. X., 2000, *ApJ*, 528, L101
- Duncan, R.A., et al., 1995, *ApJ*, 441, L73
- Gabriel, A. H., and Jordan, C., 1969, *Nature*, 221, 947
- Hillier, D. J., Davidson, K., Ishibashi, K., and Gull, T., 2001, *ApJ*, submitted
- Ishibashi, K., et al., 1999, *ApJ*, 524, 983
- Kahn, S. M., Leutenegger, M. A., Cottam, J., Rauw, G., Vreux, J. -, den Boggende, A. J. F., Mewe, R., & Güdel, M. 2001, *A&A*, 365, L312
- Kallman, T., 1995, *ApJ*, 455, 603
- Koyama, K., et al., 1990, *ApJ*, 362, 215

- Mewe, R., Kaastra, J. S., & Liedahl, D. A. 1995, *Legacy*, 6, 16
- Pittard, J. M., Stevens, I. R., Corcoran, M. F., and Ishibashi, K., 1998, *MNRAS*, 299, L5
- Schulz, N.S., Canizares, C.R., Huenemoerder, D., Lee, J.C., 2000, *ApJ*, 545, L135
- Seward, F. D., Seward, F.D., Forman, W.R., Giacconi, R., Griffiths, R.E., Harnden, F.R., Jr., Jones, C., and Pye, J.P., 1978, *ApJ*, 234, L55
- Seward, F. D., and Chlebowski, T. 1982, *ApJ*, 256, 530
- Seward, F. D., Butt, Y. M., Karovska, M., Prestwich, A., Schlegel, E. M., and Corcoran, M., 2001, *ApJ*, 553, 832
- Tanaka, Y., Inoue, H., Holt, S. S., 1994, *PASJ*, 46, L37
- Tsuboi, Y., et al., 1997, *PASJ*, 49, 85
- Usov, V. V., 1992, *ApJ*, 389, 635
- Walborn, N. R., Blanco, B. M., & Thackeray, A. D. 1978, *ApJ*, 219, 498
- Waldron, W. L. & Cassinelli, J. P. 2001, *ApJ*, 548, L45
- Weisskopf, M. C., O'Dell, S. L., & van Speybroeck, L. P. 1996, in *Proc. SPIE*, 2805, 2

Fig. 1.— Zeroth order image, color coded for X-ray energy (red - low energy; green - moderate energy; blue - high energy). The diagonal band at the top of the image is the dispersed medium energy grating (MEG) spectrum.

Fig. 2.— +1 order Medium Energy Grating (MEG) spectrum of η Carinae. Strong lines from H- and He-like ions of Mg, Si, S, Ca and Fe are indicated.

Fig. 3.— Iron K line region from the +1 order High Energy Grating (HEG) spectrum of η Carinae. Emission is seen from He-like iron originating in gas at a temperature of ~ 8 keV. In addition fluorescent line emission from cool iron is also clearly detected.

Fig. 4.— Fits to the MEG +1 order spectrum. A two-temperature fit using a variable abundance collisionally ionized plasma model (VMEKAL-XSPEC, Mewe, Kaastra & Liedahl 1995) is shown in blue, and a single-temperature fit with the same emission model is in red. The single temperature model cannot reproduce simultaneously the strength of the S XV, Si XIII and Si XIV lines in the range 4.5–7.0Å.

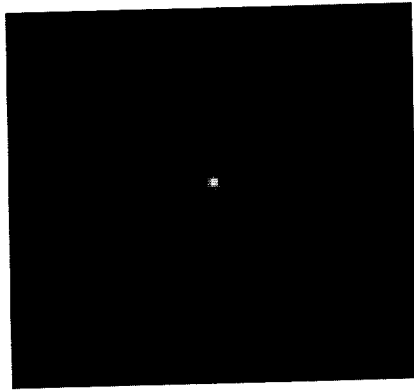
Fig. 5.— Same as in Figure 4a, but emphasizing the S & Si line region.

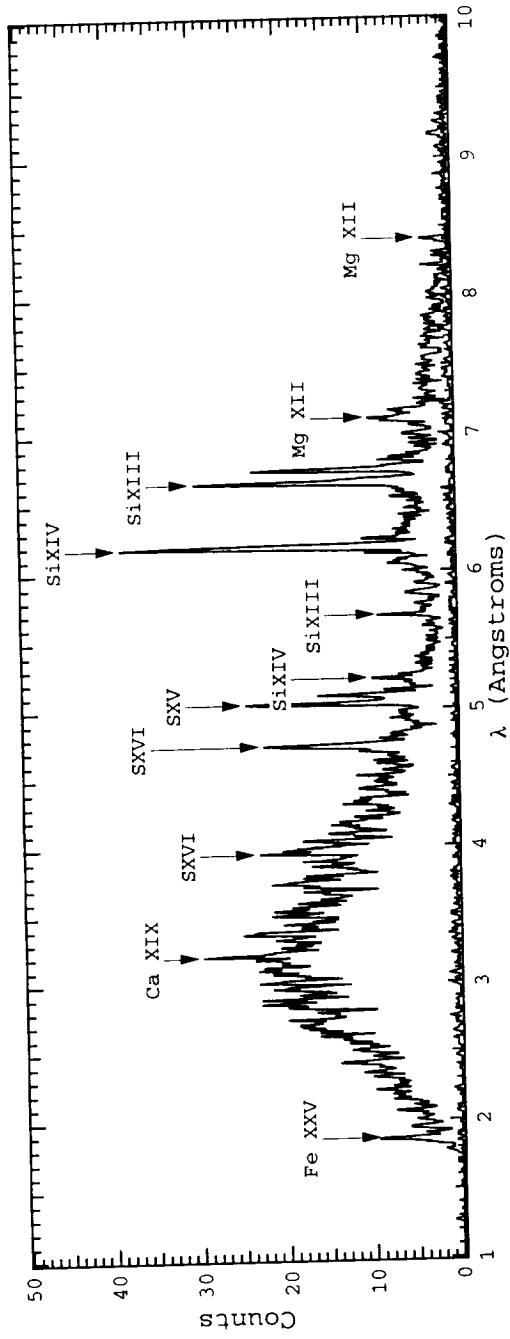
Fig. 6.— Fit to the f, i, r lines of Si XIII.

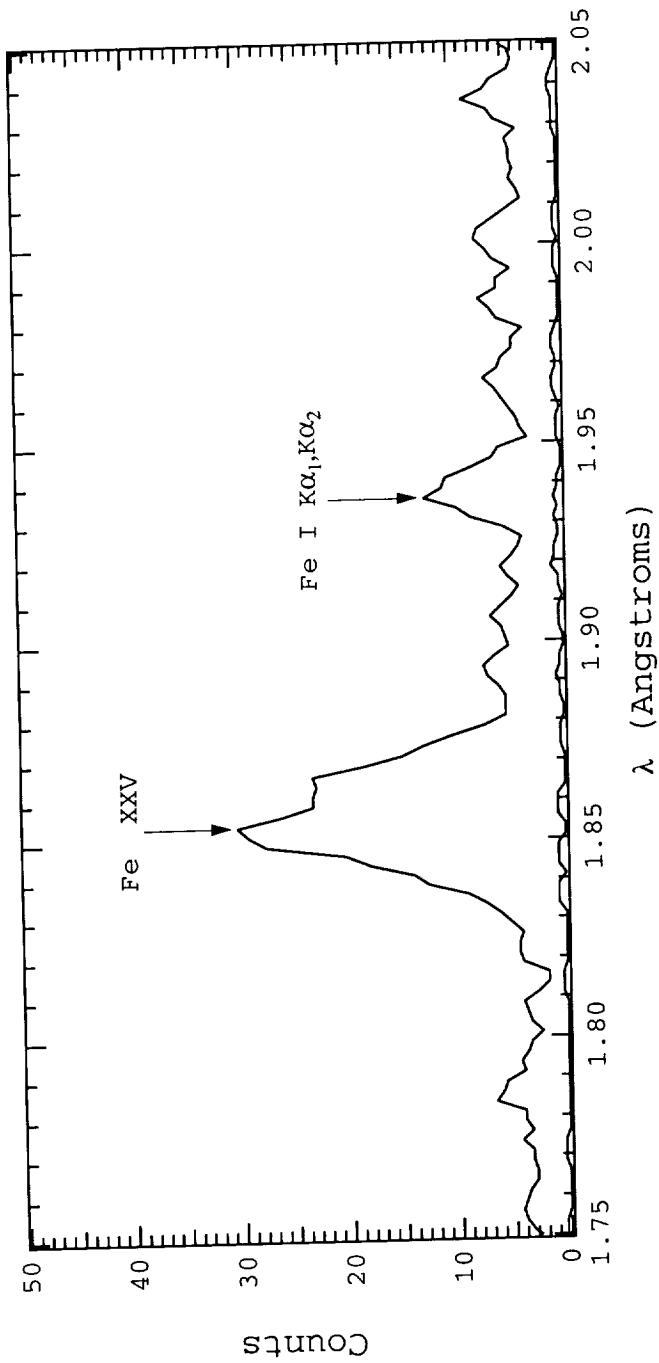
Fig. 7.— Fit to the f, i, r lines of S XV.

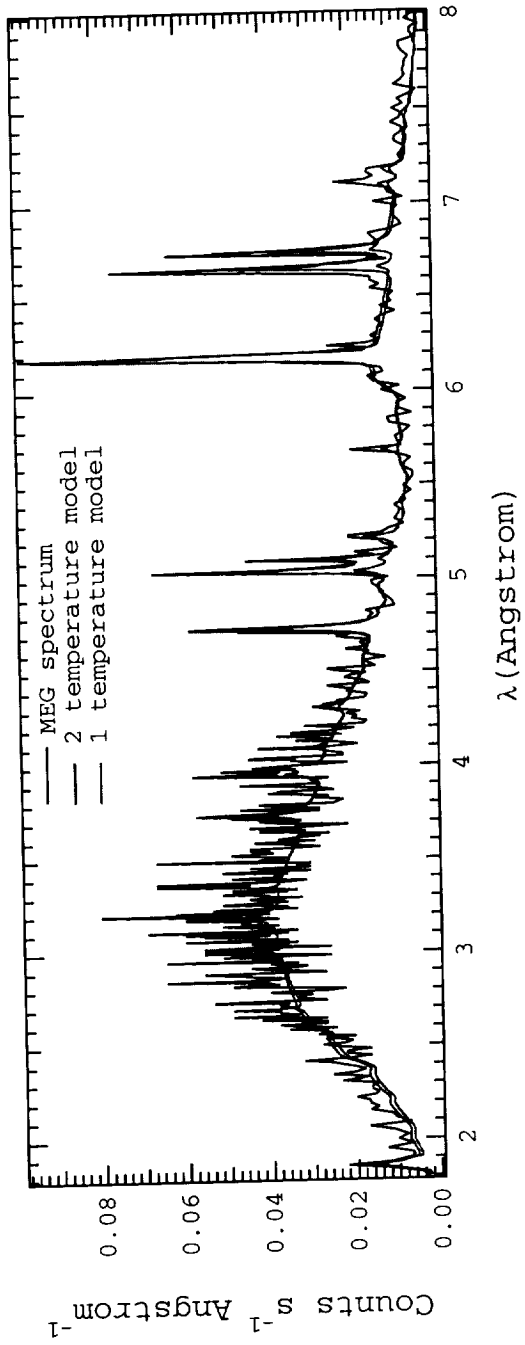
Fig. 8.— Fit to the f, i, r lines of Fe XXV (near 1.85Å) and the Fe I fluorescent line (at 1.93Å).

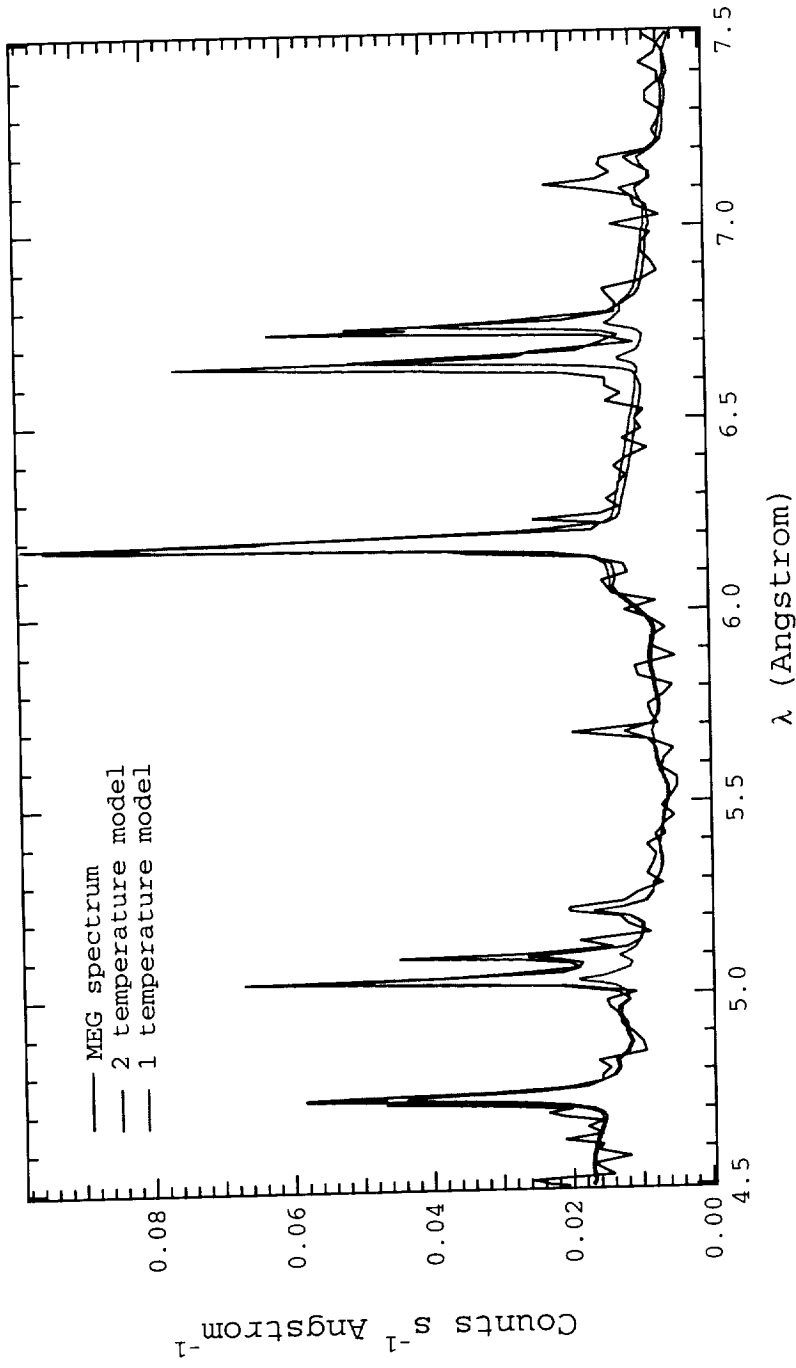
Fig. 9.— The background-corrected lightcurve of the unresolved hard source.

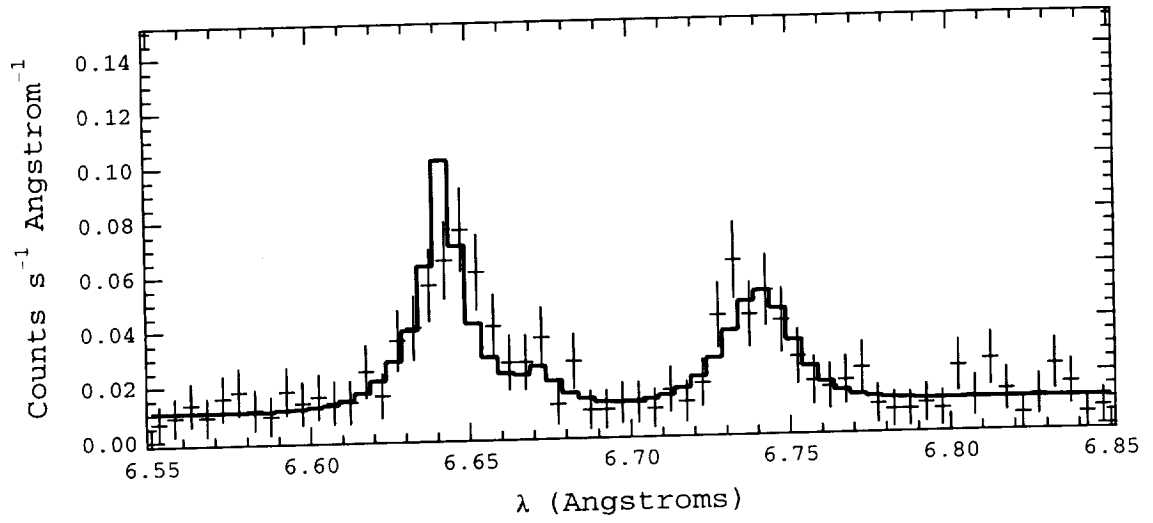


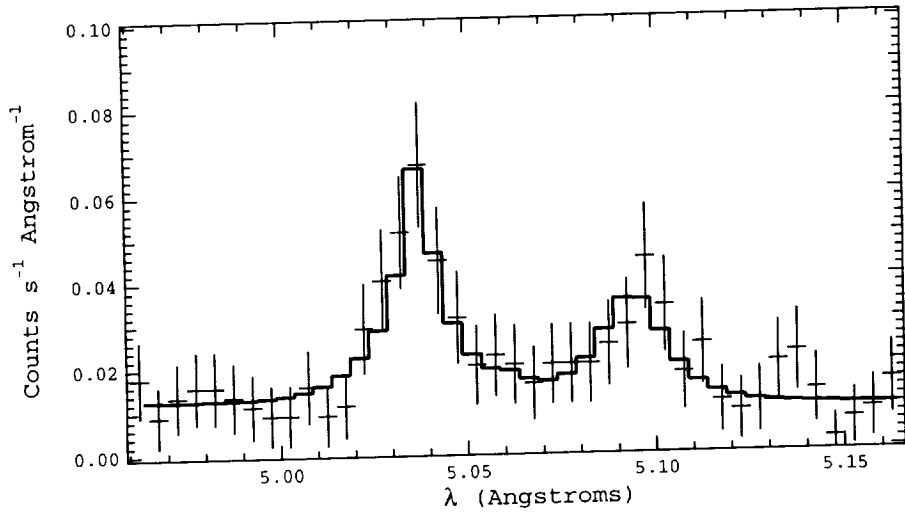


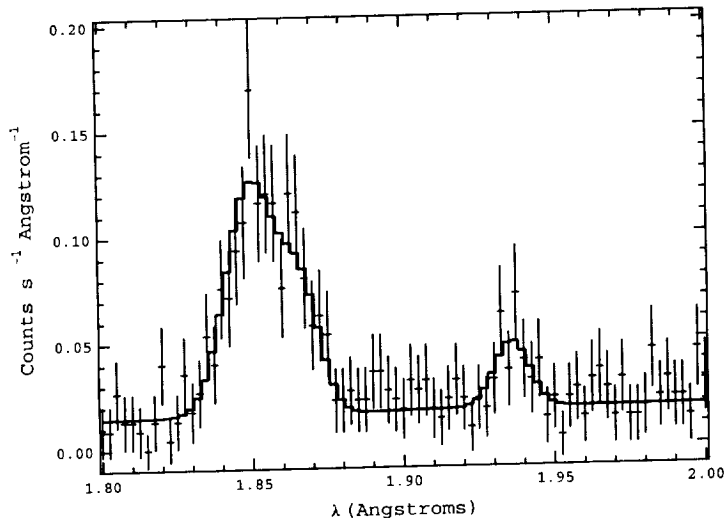


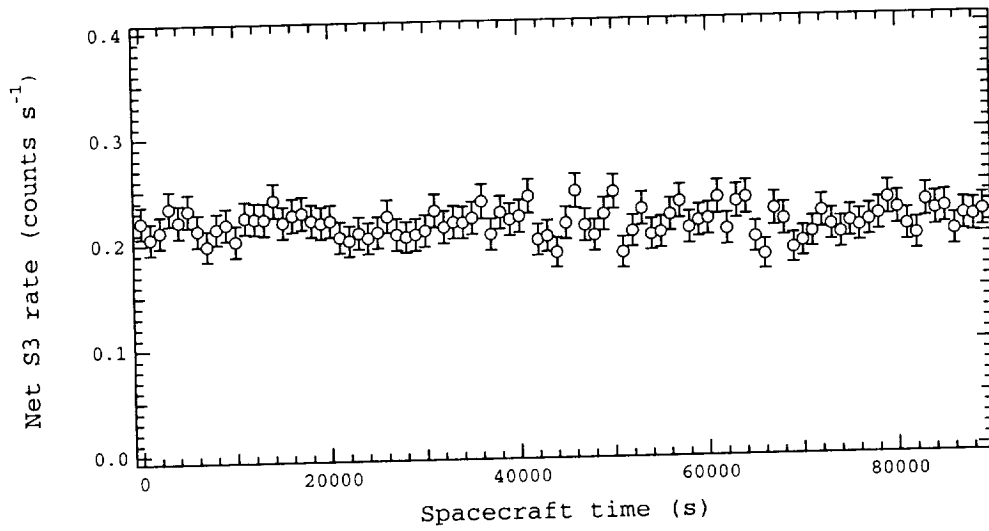












Parameter	Units	1 Component Fit	2 Component Fit
N_H	10^{22}cm^{-2}	4.9	5.1(± 0.4)
kT	keV	4.4	1.1(± 0.1)
Emission Measure ¹	10^{57}cm^{-3}	4.0	1.8(± 0.1)
Lx (2-10, absorbed) ¹	ergs s^{-1}	2.6	3.0
Lx (2-10, unabsorbed) ¹	$10^{34}\text{ergs s}^{-1}$	3.9	4.5
Si/S _⊙		1.5	1.1(± 0.2)
S/S _⊙		1.4	1.7(± 0.4)
Fe/Fe _⊙		0.6	0.9(± 0.2)
kT_2	keV		8.7(± 1.7)
Emission Measure ^{1 2}	10^{57}cm^{-3}		2.9(± 0.3)
C -statistic		2035	1619

¹ calculated assuming a distance of 2100 pc (Corcoran et al. 2001)

Line	E (keV)	Measured E (keV)	Eq. Width (eV)	Intensity (photons $s^{-1} cm^{-2} keV^{-1}$)
SiXIII (r)	1.864	1.866	38	0.017
SiXIII (i)	1.853	1.859	< 4.3	< 0.003
SiXIII (f)	1.839	1.839	21.4	0.004
SXV (r)	2.460	2.460	33.1	0.021
SXV (i)	2.450	2.450	< 6.0	< 0.003
SXV (f)	2.431	2.434	25.6	0.006
FeXXV (r)	6.700	6.700	261	0.230
FeXXV (i)	6.682	6.680	< 42	< 0.050
FeXXV (f)	6.636	6.640	42	0.100
FeI	6.424	6.407	39.4	0.055